Trapped-atom interferometer in a magnetic microtrap

W. Hänsel,* J. Reichel, P. Hommelhoff, and T. W. Hänsch
Max-Planck-Institut für Quantenoptik and Sektion Physik der Ludwig-Maximilians-Universität, Schellingstrasse 4, D-80799 München, Germany

(Received 17 June 2001; published 14 November 2001)

We propose a configuration of a magnetic microtrap that can be used as an interferometer for three-dimensionally trapped atoms. The interferometer is realized via a dynamic splitting potential that transforms from a single well into two separate wells and back. The ports of the interferometer are neighboring vibrational states in the single-well potential. We present a one-dimensional model of this interferometer and compute the probability of unwanted vibrational excitations for a realistic magnetic potential. We optimize the speed of the splitting process in order to suppress these excitations, and conclude that such interferometer device should be feasible with currently available microtrap technique.

DOI: 10.1103/PhysRevA.64.063607 PACS number(s): 03.75.−b, 39.20.+q, 39.25.+k, 03.65.−w

I. INTRODUCTION

Since the first realization of magnetic traps [1,2] and guides [3,4] with current-carrying conductors on a chip, a large variety of magnetic potentials have become experimentally accessible, which would be impractical or even impossible to realize with macroscopic coils. The splitting of two-dimensionally trapped atom clouds has been demonstrated [5,6], and recently, we were able to split and unite a three-dimensionally trapped cloud of rubidium atoms in a chip trap [7].

Current experiments aim at populating single quantum states of such microtrap potentials with either an atomic ensemble (i.e., creating a Bose-Einstein condensate), or indeed with a single atom. One promising application of such a system would be an integrated atom interferometer on a chip [8]. The small size and monolithic construction of such a device suggests its suitability for ''real-word'' applications. Moreover, the fact that magnetic potentials may be ''engineered'' on the chip enables novel interferometer schemes with features quite different from more traditional atom interferometers [9]. Here we study a scheme in which the particle wave of a single, trapped atom is coherently split up and reunited by a time-varying magnetic potential (Fig. 1). Splitting occurs in one dimension, while a tight confinement in the remaining two dimensions leads to an effective one-dimensional (1D) situation. This is in contrast to Ref. [8] where the dynamics of the splitting is in two dimensions. As depicted in Fig. 1, interference occurs between the lowest two vibrational states, $|\varphi_0\rangle$ and $|\varphi_1\rangle$, of the splitting potential (the internal atomic state remains unchanged). A phase-changing interaction in one ''arm'' (stage II in Fig. 1) translates into a change of the relative populations in $|\varphi_0\rangle$ and $|\varphi_1\rangle$ when the potential is recombined. As in other interferometers, a longer duration of stage II leads to a larger accumulated phase (i.e., a larger arm length). However, unlike the situation in most free-atom schemes and the guided-atom scheme proposed in Ref. [8], in our scheme the atom does not move nor does its wave function spread during this stage: the propagation along the traditional interferometer path is replaced by the evolution in a constant potential (stage II), which leaves the position and the physical size of the wave function unchanged. This interferometer is thus particularly well suited to measure local fields and interactions, which presents an advantage over experiments with propagating atoms.[1] One could, for instance, measure the phase shift arising from a two-body collision [11] or the amount of decoherence induced from a nearby surface [12].

In this paper, we present a detailed analysis of this interferometer scheme, employing a realisitic magnetic potential that can be implemented with currently available microtrap technique. We consider the case of an individual trapped

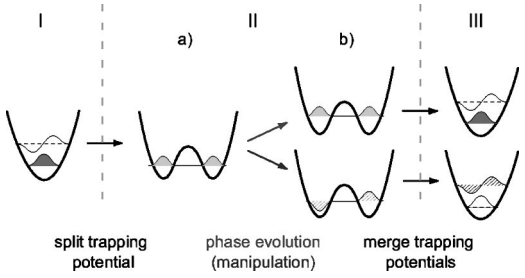

FIG. 1. Scheme of the trapped atom interferometer: one or several atoms are prepared in the vibrational ground state of the single-well potential (I). When the well separates, the wave function evolves adiabatically into a symmetric delocalized state (IIa). The phase of the wave function in each potential well can be assumed to evolve independently and monitors sensitively external electric and magnetic field gradients (IIb). As the potential wells reunite, the antisymmetric state transforms into the first excited vibrational state, whereas the symmetric one retransforms into the ground state (III).

*Corresponding author: FAX: ++49-89/285192, Email address: Wolfgang.Haensel@mpq.mpg.de

[1]There is a subtle difference between atom interferometers with beams and with trapped atoms: in spatial beam splitters, atoms are slowed down when the energy of the transverse state increases. Currently studies are on the way as to how this effect can be explored for enhanced detection schemes of the outgoing state [10].

 ©2001 The American Physical Society

atom, a situation that is also targeted by experiments under way (for a study of a Bose-Einstein condensate in an idealized 1D potential, see [13]). The potential is created by the simple conductor configuration shown in Fig. 2. The current I_0 together with the external field $B_{0,y}$ provides a tight confinement in the yz plane. The two currents I_{ext} together with the homogeneous field component $B_{0,x}$ close this 2D trap in axial direction, completing the single-well potential [Fig. 3(a), left]. The current I_c creates an adjustable ''bump'' in the center of this trap, and thus induces the splitting. Increasing I_c transforms the potential from single-well to double-well [Fig. 3(a), right], in loose analogy with the first passage through the beam splitter of a Michelson-Moreley interferometer for light.

To achieve a good fringe contrast, it is essential that no higher-lying vibrational states be excited during this splitting. Therefore, the crucial part of the interferometer is the quantum dynamics during the splitting and merging process. The splitting (merging) of the wave functions occurs as the quantum states adiabatically evolve in the varying potential. We analyze these dynamics in a one-dimensional model, using analytic expressions for the microtrap magnetic field. We numerically determine the energy eigenstates of ^{87}Rb atoms in the given potential and then trace the dynamics of an initial state, using the eigenstates as a time-dependent basis.

We show that successive vibrational levels in the initial trap evolve into pairs of degenerate states when the potential is split. In this ''sensing state,'' the wave functions are composed of two identical oscillator states in the left and in the right well. Either of the two parts can acquire a phase shift independent of the other one, reflecting, e.g., an additional small field gradient or the presence of an additional atom in one of the wells. When the potential is transformed back into a single well, the population of the vibrational levels depends on the phase difference that is picked up in the degenerate states. Figure 1 illustrates this process: first, the system (i.e., one or several atoms) is prepared in the vibrational ground state. Upon separation of the potential, this state evolves into a symmetric state that spreads over the two potential wells. In an analogous manner, the antisymmetric first vibrational level transforms into an antisymmetric delocalized state. As the system's Hamilton operator is symmetric throughout the whole process, it cannot induce transitions between states of opposite symmetry, and the eigenstates can always be chosen of well-defined parity.

If the symmetric and antisymmetric states are spatially separated far enough, they degenerate, and the left (right) localized state can be constructed as difference (sum) of the symmetric and antisymmetric states. A perturbation of the potential, which does not have even parity, will lift this degeneracy in favor of the localized states. These localized states make up for the classical interferometer arms, measuring very sensitively deviations from an ideal symmetric potential or interactions with other atoms.

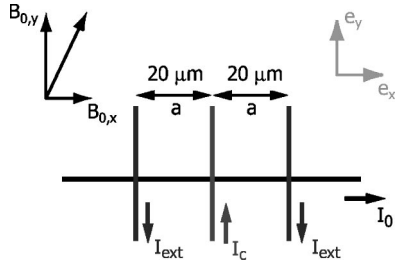

FIG. 2. Layout of the interferometer conductor pattern.

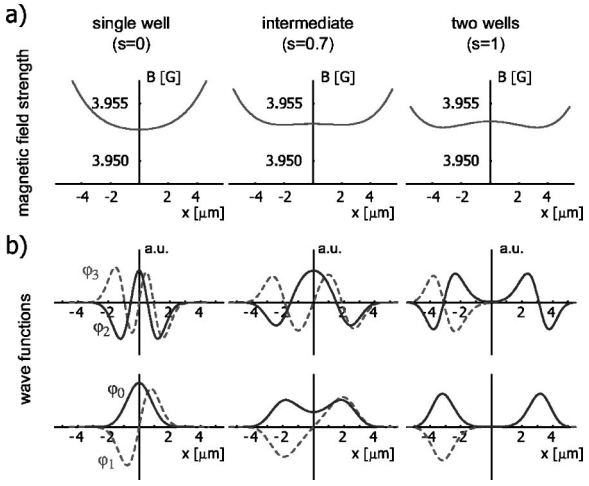

FIG. 3. (a) Shape of the magnetic splitting potential for characteristic values of the control parameter s [see Eqs. (4) and (5)]; (b) eigenstates of ^{87}Rb atoms in the specified potential.

In the following section, we investigate the separation process using the 1D potential taken from the microtrap device sketched in Fig. 2. We establish the quantum-mechanical equation of motion and use first-order perturbation theory to determine the amount of vibrational excitations. Assuming a linear variation of the current I_c, we find the excitation probability lower than 1% if the separation takes 60 ms or longer. This indicates that an experimental realization should be possible, and the situation can still be improved when an arbitrary variation of I_c is allowed. We, therefore, dedicate Sec. III to a method that minimizes nonadiabatic excitations by finding the most-appropriate time dependence for the shape of the potential (here controlled via I_c). Such method is of interest not only for interferometers, but it also applies to all cases of time-dependent potentials, and it can even be transferred to spatially varying potentials such as beam splitters. For our interferometer, this method helps to reduce the splitting time by a factor of 2, at the same time reducing the excitation probability by more than a factor of 10.

II. THE TRAPPED ATOM INTERFEROMETER

The microtrap device that we propose for the interferometer is a symmetric arrangement of wires as depicted in Fig. 2. Its potential is similar to the one that we used in the merging experiment with thermal atoms [7], but it is scaled down to a wire distance of 20 μm and simplified to produce a strictly symmetric potential. The quantum-state computations are made for ^{87}Rb atoms in the $|F=2,m_F=2\rangle$ ground state, the effective potential being $U(x) \approx h \times (1.4\ \mathrm{MHz}) \times B_{\min}(x)$, where $B_{\min}(x)$ is the transverse minimum of the magnetic field amplitude and is measured in gauss.

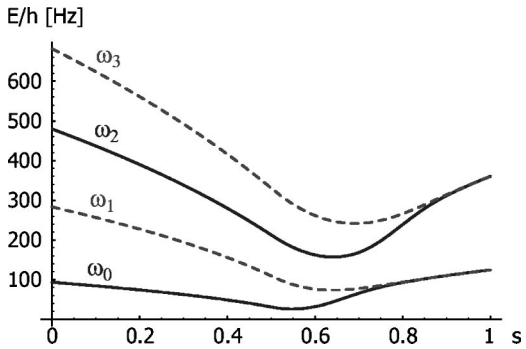

FIG. 4. Energy eigenvalues of the system's Hamilton operator as the trapping potential is divided into two wells. Neighboring states of opposite symmetry form pairs and degenerate as the potential wells separate.

The current I_0 in the central wire and the homogeneous field $B_{0,y}$ create a two-dimensional quadrupole field that strongly confines the atoms in the yz plane. Each of the crossing wires contributes a longitudinal field modulation of Lorentzian shape (see [14]).

The two currents I_{ext} together with the field component $B_{0,x}$ generate two valleys along the longitudinal axis, which do not appear separate if the trap is located far enough from the surface. The current I_c with its direction opposite to the two external currents is used to split the Ioffe-Pritchard potential into two neighboring wells [Fig. 3(a)]. Choosing the parameters as

$$I_0 = 525 \text{ mA}, \tag{1}$$

$$B_{0,y} = 20 \text{ G}, \tag{2}$$

$$B_{0,x} = 16 \text{ G}, \tag{3}$$

$$I_{ext} = 140 \text{ mA} + (2.91 \text{ mA}) \times s, \tag{4}$$

$$I_c = 0.25 \text{ mA} + (4.4 \text{ mA}) \times s, \tag{5}$$

the trap is located 35 μm above the surface, yielding a transversal oscillation frequency of $\omega_{trans} \approx 2\pi \times 53.7$ kHz. The parameter s determines the shape of the trap, running from 0 for one single well to 1 for separated wells. The point $s=1$ has been chosen such that the two lowest vibrational levels of each well are clearly separated (i.e., the two lowest sets of states are both degenerate). The time dependence of the system's Hamiltonian is expressed via the function $s(t)$. In a simple approach, s may be chosen to vary linearly in time, but as we will discuss in Sec. III, an optimized function $s(t)$ can be found that minimizes vibrational excitations during the splitting (merging) process.

In Fig. 3(a), the resulting magnetic field along the longitudinal axis $\mathbf{e}_x$ is displayed for characteristic values of s; the transverse potential minimum is plotted against the longitudinal position. The plots below show the eigenstates of ^{87}Rb atoms ($|F=2, m_F=2\rangle$) in this field as they are numerically computed from the Schrödinger equation [Eq. (6) below]. The corresponding energy eigenvalues, measured relative to the minimum value of the potential, are given in Fig. 4.

For $s=0$, the four lowest levels correspond to the states of a harmonic oscillator with quantum number $n=0,\ldots,3$ and oscillation frequency $\omega_{s=0} \approx 2\pi \times (190 \text{ Hz})$. We use the quantum number n to identify the eigenstates as $|\varphi_n(s)\rangle$ throughout the whole evolution. As the value of s is raised, the vibrational levels evolve into symmetric and antisymmetric delocalized states. At $s=1$, the four lowest levels form two sets of degenerate states, their energy being $E_{2k} = E_{2k+1} = \hbar\omega_{s=1}(k+\frac{1}{2})$, $k=\{0,1\}$, $\omega_{s=1} \approx 2\pi \times (240 \text{ Hz})$. At each stage, the separation of the transverse levels (>50 kHz) is much larger than the separation of longitudinal states involved. For this reason, the longitudinal states do not intermingle with the transverse levels, even if the system's symmetry is slightly disturbed. The quantum dynamics is, therefore, adequately described by a one-dimensional model.

In order to make the interferometer work properly, the atomic wave function should follow ideally the (time-dependent) eigenstates $|\varphi_k(t)\rangle$ of the system. If the potential is varied too fast, the evolution is nonadiabatic, i.e., vibrational excitations are generated. For the investigation of these excitations, we will focus on the first half of the interferometer cycle: we use a time-dependent interaction picture to compute the time scale on which the separation process can be lead adiabatically.

The (time-dependent) basis for the computation is found by solving the time-independent Schrödinger equation

$$\hat{H}(s)|\varphi_k(s)\rangle = \hbar\omega_k(s)\,|\varphi_k(s)\rangle \tag{6}$$

with the Hamilton operator

$$\hat{H}(s) = \frac{\hat{\mathbf{p}}^2}{2m} + \mu_B g_F m_F |\mathbf{B}(s, \hat{\mathbf{r}})|, \tag{7}$$

where s takes the role of a mere parameter. For the given magnetic-field, the eigenfunctions have been computed numerically and are displayed in Fig. 3(b).

The natural phase evolution of the eigenstates can be included into the basis and yields the ansatz

$$|\psi(t)\rangle = \sum_k c_k(t) \exp\left[-i\int_0^t \omega_k(t')\,dt'\right]|\varphi_k(t)\rangle. \tag{8}$$

The equation of motion for the coefficients $c_k(t)$ is obtained when Eq. (8) is inserted in the time-dependent Schrödinger equation with the Hamiltonian (7)[2]

$$\frac{d}{dt}c_k(t) = -\sum_n c_n(t) \exp\left\{i\int_0^t [\omega_k(t') - \omega_n(t')]dt'\right\} \times \langle\varphi_k(t)|\frac{d}{dt}|\varphi_n(t)\rangle. \tag{9}$$

[2]The time dependence of $\omega_k(t)$ and $|\varphi_k(t)\rangle$ is explicit through the control parameter s: $\omega_k(t) \equiv \omega_k(s(t))$, etc.

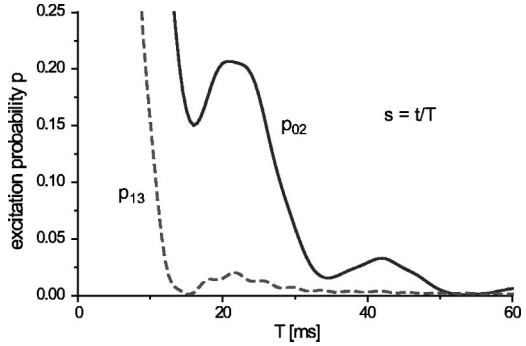

FIG. 5. Excitation probability for the transitions $|\varphi_0\rangle \rightarrow |\varphi_2\rangle$ and $|\varphi_1\rangle \rightarrow |\varphi_3\rangle$ for a linear increase of the separation s with time.

Given that a single eigenstate $|\varphi_i(t=0)\rangle$ is prepared in the beginning, and further assuming that the transition probability into other vibrational states is small, first-order perturbation theory can be used to determine the coefficients c_f and the corresponding transition probabilities P_{if}

$$c_f(t) = \int_0^t \exp\left\{ i \int_0^t [\omega_f(t') - \omega_i(t')] dt' \right\} \times \langle \varphi_f(t) | \frac{d}{dt} | \varphi_i(t) \rangle \, dt \tag{10}$$

$$P_{if}(t) = |c_f(t)|^2. \tag{11}$$

The coupling

$$\langle \varphi_f(t) | d/dt | \varphi_i(t) \rangle = \langle \varphi_f(s) | d/ds | \varphi_i(s) \rangle \, ds/dt$$

to higher levels is directly proportional to the rate ds/dt at which the control parameter s is changed. Therefore, if all levels are separated by a minimum energy $\hbar\omega_0$, the transition amplitudes can be made negligible by choosing an appropriate duration for the process. Conversely, if at certain instants some energy levels degenerate, this will create large transition amplitudes unless the coupling coefficient $\langle \varphi_f(s) | d/ds | \varphi_i(s) \rangle$ between these levels vanishes at the points of degeneration. In the trapped atom interferometer presented here, we encounter such degenerate levels. But as the states that degenerate are of opposite symmetry throughout the complete evolution, the coupling between them remains zero for all times. Therefore, the excitation probability can be made arbitrarily small by choosing the process duration long enough.

This consideration is confirmed by numerically evaluating expressions (10) and (11) for either of the interferometer levels $(|\varphi_0\rangle, |\varphi_1\rangle)$. In the first approach, the separation parameter has been chosen linear in time $s = t/T$. Figure 5 shows the transition probabilities into the neighboring interferometer levels which contribute largest to all vibrational excitations. The data indicate that the excitation probability is less than 1% if the separation process takes longer than 60 ms.

This is an encouraging result, as it seems experimentally realizable. Moreover, as the time dependence of the potential can be freely chosen, one can adjust the speed of the separation process ds/dt in order to further reduce excitations. This is of general interest, because a linear variation of the control parameter s is not necessarily the best choice. Indeed, one wishes to find a method that optimizes the process irrespective of its parametrization.

III. OPTIMIZATION

In this section, we develop a scheme that minimizes vibrational excitations in time-dependent potentials. In a slight variant, this method can equally be used to find an adequate shape for a beam-splitter potential.

In order to optimize the adiabaticity of the separation process we first take a look at the coupling term from Eq. (10)

$$\langle \varphi_f(t) | \frac{d}{dt} | \varphi_i(t) \rangle = \langle \varphi_f(s) | \frac{d}{ds} | \varphi_i(s) \rangle \frac{ds}{dt}, \tag{12}$$

which is proportional to the process speed ds/dt and to the coupling coefficient $a(s) \equiv \langle \varphi_f(s) | d/ds | \varphi_i(s) \rangle$.

Intuitively, one can increase the process speed ds/dt if $a(s)$ is small, and decrease it in the opposite case. Furthermore, the process speed should be adapted to the energy difference of the levels involved; the more the energy levels lie apart from each other, the more the process speed may be increased. Last but not the least, one has to avoid discontinuities in the process speed including the start and the end of the separation. In the following, these intuitive rules will be substantiated into a set of differential equations to yield an optimized process control $s(t)$.

We assume that the process is lead during $0 \leqslant t \leqslant T$ and that the separation parameter at $t = T$ is $s(t=T) = 1$. Indeed, we want to fix a shape of the control parameter s that does not depend on the process duration. Therefore, we implicitly assume that $s(t) \equiv s(t,T)$ can be written as

$$s(t,T) = s(t/T, 1). \tag{13}$$

The goal is then to fix some maximum excitation probability ϵ^2 and to find an appropriate shape for the function $s(t,T)$ which minimizes T_{adiab} fulfilling the condition

$$|c_f(T)| \leqslant \epsilon \quad \forall \; T \geqslant T_{\text{adiab}}. \tag{14}$$

If, by some chance, the distance of energy levels $\Delta\omega(s(t')) \equiv \omega_f - \omega_i$ is constant throughout the process, the transition amplitude $c_f(T)$ appears as the Fourier transform of $a(s)\, ds/dt$,

$$c_f(T) = \int_0^T \exp\left[i \int_0^t \Delta\omega(t')\, dt' \right] a(s(t)) \frac{ds}{dt} dt \tag{15}$$

$$= \int_0^T e^{i\Delta\omega t} a(s) \frac{ds}{dt} dt \quad \text{for } \Delta\omega = \text{const.} \tag{16}$$

If, in addition, $a(s)$ happens to be constant over the process, the solution of the problem is simple: the shape of the process speed ds/dt should be chosen such that it produces the

least amount of side lobes possible in a Fourier transformation. An appropriate shape would, e.g., be a Blackman pulse [15]:

$$\frac{ds}{dt}=\frac{1}{T}\left[1-\frac{25}{21}\cos\left(2\pi\frac{t}{T}\right)+\frac{4}{21}\cos\left(4\pi\frac{t}{T}\right)\right], \quad (17)$$

which can be directly integrated to yield $s(t)$.

The idea of the Fourier transform can be extended to the more general case. A substitution of the time variable t by some new variable τ can be made in a way that the argument of the exponential in Eq. (15) becomes linear in τ

$$\int_0^t \Delta\omega(t')\,dt'=\frac{T}{T_0}\tau(t), \quad (18)$$

and that τ runs from 0 to 1 during the process. The time scale T_0 will be part of the optimization result. Equation (15) then assumes the form of a Fourier transform of some new expression[3] $u(\tau)$,

$$c_f(T)=\int_0^1 \exp\left[i\frac{T}{T_0}\tau\right]u(\tau)\,d\tau, \quad (19)$$

$$u(\tau)\equiv a(s)\frac{ds_\tau}{d\tau}. \quad (20)$$

The expression $u(\tau)$ is a generalized coupling term, acting in the transformed time frame τ. As above, one can now choose a shape for this coupling term $u(\tau)$ (however, not its amplitude) and will obtain the probability amplitude as its Fourier transform.

Once the optimization strategy is chosen, it remains to solve the equations (18) and (20). One might be tempted to deduce the relation $dt/d\tau$ from Eq. (18) and insert it into Eq. (20) to solve directly for $s(t)$. Unfortunately, this results in an intractable problem. Instead, one can take advantage of the substitution already made and first solve for $s_\tau(\tau)$. The relation between τ and t is then established in a second step. This way, the problem is split into two differential equations, the first of which yields the amplitude of $u(\tau)$, and the second of which determines the time scale T_0 used in the substitution. These two values determine size and scale of the probability amplitude $c_f(T)$.

The first differential equation involves the shape of the function that is chosen for the generalized coupling term $u(\tau)$, and it is a direct consequence of Eq. (20),

$$\frac{ds_\tau}{d\tau}=\frac{u(\tau)}{a(s_\tau(\tau))}. \quad (21)$$

It is important to note, that although the time $ds_\tau/d\tau$ is used to shape the coupling term $u(\tau)$, its amplitude does not correspond to the overall process speed. Instead, the amplitude of $u(\tau)$ has to be adjusted such that the solution matches the boundary conditions $s(\tau=0)=0$, $s(\tau=1)=1$. This can for instance be done by iteratively solving Eq. (21) for different amplitudes of $u(\tau)$.

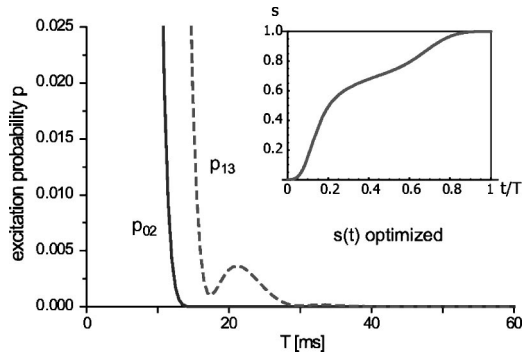

FIG. 6. Excitation probability $|\varphi_0\rangle\rightarrow|\varphi_2\rangle$ and $|\varphi_1\rangle\rightarrow|\varphi_3\rangle$ for an optimized process $s(t)$ (see inset). Note that the ordinate is scaled up by a factor of 10 compared to Fig. 5.

The second differential equation establishes the relation between t and τ and arises from the substitution of t [Eq. (18)], once that $s_\tau(\tau)$ has been determined,

$$\frac{d\tau}{dt}=\Delta\omega(s_\tau(\tau))\frac{T}{T_0}. \quad (22)$$

Choosing $T=T_0$, this equation can be solved numerically, and one finds T_0 as the point in time, for which $\tau(t)$ reaches its boundary $\tau(T_0)=1$.

The result for the transition amplitude is now completely described by Eq. (19), the amplitude of $u(\tau)$, and the time scale resulting from the choice of the pulse shape. The optimized evolution of the control parameter is computed from the concatenation of $s_\tau(\tau)$ and $\tau(t)$,

$$s(t)=s_\tau\left(\tau\left(t\frac{T_0}{T}\right)\right). \quad (23)$$

If this optimization is applied to the trapped atom interferometer, the probability for nonadiabatic excitations can be considerably reduced. Figure 6 shows the excitation probabilities for a process speed that has been optimized to suppress the transition $|\varphi_0\rangle\rightarrow|\varphi_2\rangle$. With the optimized control, the separation can be accomplished within 30 ms, thus reducing the complete interferometer cycle to 60 ms with an overall excitation probability of less than 10^{-3}.

These parameters suggest that an experimental realization of the scheme is indeed feasible. Direct Bose-Einstein condensation in microtraps, which has been demonstrated very recently [16,17], can be used to provide an initial atomic sample in the vibrational ground state. The density in the condensate has to be reduced such that phase shifts from the mean-field interaction are avoided. With a sufficient number of atoms, one can determine the final state from the atomic velocity distribution using time-of-flight imaging [18]. Alternatively, the interferometer output can be determined after spatial separation of the final states, e.g., using appropriate potential changes as proposed in Ref. [8]. For sensitive detection, one could then use established techniques such as fluorescence imaging.

[3]In the following equations, the index τ marks the fact that the functional dependence of the parameter s is on τ, not on t.

Another issue is stability against gradients of magnetic stray fields. In our case, the sensing states of the interferometer lie ~ 6 μm apart. During a sensing time of 60 ms, a gradient $b_x = \partial B_x / \partial x$ would lead to an additional dephasing of $\Delta\Phi \approx 2\pi \times 50 \times b_x$, where b_x is measured in G/cm. A suppression of stray gradients to less than 1 mG/cm would, therefore, reduce the dephasing to $\Delta\phi \leqslant 2\pi/20$.

IV. CONCLUSION

In conclusion, we have studied a dynamic potential interferometer working with three-dimensionally trapped atoms. We have used a time-dependent interaction picture to describe the quantum-state evolution and we have computed probabilities for nonadiabatic transitions into neighboring levels. For a realistic magnetic microtrap we find parameters that suggest an experimental implementation in the near future. Based on the theoretical results, we have developed an optimization scheme for the reduction of vibrational excitations that is independent of the system's parametrization. Applying the optimization to our interferometer potential, we have found a cycle of duration $T = 60$ ms with excitation probability less than 10^{-3}.

[1] J. Reichel, W. Hänsel, and T.W. Hänsch, Phys. Rev. Lett. **83**, 3398 (1999).

[2] R. Folman, P. Krüger, D. Cassettari, B. Hessmo, T. Maier, and J. Schmiedmayer, Phys. Rev. Lett. **84**, 4749 (2000).

[3] D. Müller, D.Z. Anderson, R.J. Grow, P.D.D. Schwindt, and E.A. Cornell, Phys. Rev. Lett. **83**, 5194 (1999).

[4] N.H. Dekker, C.S. Lee, V. Lorent, J.H. Thywissen, S.P. Smith, M. Drndič, R.M. Westervelt, and M. Prentiss, Phys. Rev. Lett. **84**, 1124 (2000).

[5] D. Müller, E.A. Cornell, M. Prevedelli, P.D.D. Schwindt, A. Zozulya, and D.Z. Anderson, Opt. Lett. **25**, 1382 (2000).

[6] D. Cassettari, B. Hessmo, R. Folman, T. Maier, and J. Schmiedmayer, Phys. Rev. Lett. **85**, 5483 (2000).

[7] W. Hänsel, J. Reichel, P. Hommelhoff, and T.W. Hänsch, Phys. Rev. Lett. **86**, 608 (2001).

[8] E.A. Hinds, C.J. Vale, and M.G. Boshier, Phys. Rev. Lett. **86**, 1462 (2001).

[9] P.R. Berman, *Atom Interferometry* (Academic Press, San Diego, 1997).

[10] Erika Andersson, Tommaso Calarco, Ron Folman, Mauritz Andersson, Björn Hessmo, and Jörg Schmiedmayer, e-print quant-ph/0107124.

[11] T. Calarco, E.A. Hinds, D. Jaksch, J. Schmiedmayer, J.I. Cirac, and P. Zoller, Phys. Rev. A **61**, 022304 (1999).

[12] C. Henkel, S. Potting, and M. Wilkens, Europhys. Lett. **47**, 414 (1999).

[13] C. Menotti, J. Anglin, J. Cirac, and P. Zoller, Phys. Rev. A **63**, 023601 (2001).

[14] J. Reichel, W. Hänsel, P. Hommelhoff, and T.W. Hänsch, Appl. Phys. B: Lasers Opt. **72**, 81 (2001).

[15] R.B. Blackman and J.W. Tukey, *The Measurement of Power Spectra from the Point of View of Communications Engineering* (Dover Publications, New York, 1958).

[16] H. Ott, J. Fortagh, G. Schlotterbeck, A. Grossmann, and C. Zimmermann, Phys. Rev. Lett. (to be published).

[17] W. Hänsel, P. Hommelhoff, T.W. Hänsch, and J. Reichel, Nature (London) **413**, 498 (2001).

[18] I. Bouchoule, H. Perrin, A. Kuhn, M. Morinaga, and C. Salomon, Phys. Rev. A **59**, R8 (1999).